AIMS Mathematics, 10(8): 18381–18397.
DOI: 10.3934/math.2025821
Received: 05 June 2025
Revised: 31 July 2025
Accepted: 01 August 2025
Published: 13 August 2025

https://www.aimspress.com/journal/Math

Research article

Robin-Schwarz algorithm for contact conductance heat transfer

Huan Zhang and YingXiang Xu*

School of Mathematics and Statistics, Northeast Normal University, Changchun 130024, China

* **Correspondence:** Email: yxxu@nenu.edu.cn.

Abstract: This paper explored the optimized Schwarz method (OSM) for solving contact conductance heat transfer problems, with a particular emphasis on the impact of thermal contact resistance (TCR) on the convergence behavior of the OSM algorithm when the standard Robin transmission condition is applied. The presence of TCR introduces a challenging optimization problem, which was rigorously addressed to determine the optimal Robin parameter and describe the corresponding convergence behavior. Our analysis yielded several novel findings. First, an increase in TCR results in faster convergence of the OSM algorithm. Second, mesh-independent convergence was achieved in an asymptotic sense, contrasting with the mesh-dependent convergence observed in the absence of TCR. Third, unlike the deceleration caused by strong heterogeneity in the TCR-free scenario, increased heterogeneity contrast accelerates convergence. Thermal conductivity also contributes to convergence enhancement in a manner analogous to the effect of heterogeneity. These theoretical results were validated through numerical experiments, demonstrating the significant influence of TCR on the performance of the OSM algorithm in contact conductance heat transfer problems.

Keywords: optimized Schwarz method; contact conductance heat transfer; thermal contact resistance; domain decomposition; optimized transmission condition
Mathematics Subject Classification: 65M55

1. Introduction

Heat transfer across the interface between two solids plays a critical role in numerous engineering applications, including aerospace [1] and electronics [2]. The interfacial conditions are strongly influenced by the degree of contact at the interface. Under perfect contact conditions, the temperature and heat flux remain continuous across the interface [3]. However, due to the inherent roughness of real surfaces, complete contact is unattainable, leading to the formation of voids. These voids give rise to thermal contact resistance (TCR), also referred to as "Kapitza" resistance [4], which is defined as the reciprocal of thermal contact conductivity. The presence of TCR introduces discontinuities in

the interfacial temperature, resulting in jumps in the interfacial conditions. Consequently, accurate modeling of heat transfer with TCR is essential for practical simulations.

The contact conductance heat transfer can be mathematically modeled as follows. Denote by $\Omega := \Omega_1 \cup \Omega_2$ an open bounded domain in $\mathbb{R}^d$, $d = 1, 2, 3$, with a Lipschitz continuous boundary $\partial\Omega$. The two adjacent subdomains Ω_1 and Ω_2 are bounded domains occupied by different media whose thermal properties could be distinct, satisfying $\Omega_1 \cap \Omega_2 = \emptyset$. The interface between these subdomains is denoted by $\Gamma := \partial\Omega_1 \cap \partial\Omega_2$. The governing equations describe the steady-state heat transfer while the interface condition ensures the continuity of heat flux across Γ, where the temperature difference between subdomains is proportional to the heat flux, with TCR serving as the proportionality coefficient. The temperature field T then satisfies the following partial differential equation [5] and interface conditions [6]:

$$\begin{cases} -\nabla \cdot (\kappa(x)\nabla)T + c(x)T = f & \text{in } \Omega, \\ T = 0 & \text{on } \partial\Omega, \\ \kappa_1 \nabla T_1 \cdot \mathbf{n_1} = -\kappa_2 \nabla T_2 \cdot \mathbf{n_2} & \text{on } \Gamma, \\ T_1 - T_2 = R_c \kappa_2 \nabla T_2 \cdot \mathbf{n_2} & \text{on } \Gamma, \end{cases} \tag{1.1}$$

where $T_i = T|_{\Omega_i}$, and the thermal conductivity $\kappa(x)$ and the reaction coefficient $c(x)$ are piecewise constant functions

$$\kappa(x) = \begin{cases} \kappa_1 & \text{in } \Omega_1, \\ \kappa_2 & \text{in } \Omega_2, \end{cases} \qquad c(x) = \begin{cases} c_1 & \text{in } \Omega_1, \\ c_2 & \text{in } \Omega_2, \end{cases}$$

with $\kappa_i > 0$ and $c_i \geq 0$ for $i = 1, 2$. Note that $c_i > 0$ is associated with the reciprocal of the time step size when addressing time-dependent problems through a time-marching scheme. The function f represents a given source term. $\boldsymbol{n_i}, i = 1, 2$, denotes the unit normal vector pointing outward on Ω_i. We here comment that when $R_c = 0$, the interface condition in (1.1) degenerates to a continuous interface condition.

Both analytical [7–9] and numerical methods [10–12] are widely employed to solve elliptic problems with perfect contact interfaces. Although the case presenting TCR has attracted some attention [13–15], the research is still quite limited. Analytical approaches often rely on restrictive geometric and boundary assumptions, limiting their applicability to complex scenarios. In contrast, the monolithic numerical methods, though more flexible, can suffer from ill-conditioned systems due to material heterogeneity, leading to non-physical oscillatory behavior. The heterogeneous domain decomposition method [16] effectively addresses these challenges by partitioning the domain according to the spatial variation of material properties. This approach enables the use of established physical solvers in an iterative framework, enhancing computational efficiency and mitigating non-physical oscillations.

The optimized Schwarz method (OSM), compatible with non-overlapping subdomains (as demonstrated in [17]), is particularly well-suited for heterogeneous domain decomposition. The OSM has achieved notable success in solving steady-state problems in heterogeneous domains, including Helmholtz-Laplace coupling [18], Stokes-Darcy coupling [19–21], and the coupling of second-order elliptic partial differential equations (PDEs) [22], as well as problems with discontinuous coefficients [23]. Notably, Dubois and Gander [23] developed four optimized transmission conditions for the non-overlapping OSM applied to steady-state thermal diffusion models with discontinuous

coefficients: standard Robin, scaled Robin, two-sided Robin, and Ventcel conditions. The results indicate that the standard Robin condition leads to mesh-dependent convergence of the OSM algorithm, and more importantly, it suffers from the large heterogeneity contrast. In comparison, this heterogeneity contrast benefits the convergence when the other three transmission conditions are applied.

Since the construction of the standard Robin condition is very natural in applications, in this work, we focus on the OSM algorithm using the standard Robin condition to solve the contact conductance heat transfer problem. The presence of TCR significantly increases the difficulty in determining the optimal parameters: the interior maxima points with respect to the Fourier frequencies, arising during the minimization of the supremum of the convergence factor over all Fourier frequencies, typically lack explicit closed-form expressions. This poses a formidable challenge to theoretical analysis. This work partially solves this problem and provides a theoretical solution to this optimization problem under specific conditions. Theoretically, the results show that, unlike the case without TCR, the large heterogeneity contrast also benefits the convergence of the standard Robin condition, leading to mesh-independent convergence similar to the scaled Robin condition [24]. The convergence also benefits from the existence of the TCR directly: the larger the TCR, the faster the algorithm converges.

The paper is organized as follows. In Section 2, we introduce the OSM algorithm to solve the problem and provide a Fourier analysis-based convergence result when the standard Robin transmission condition is applied. Section 3 focuses on optimizing Robin parameters, including a comparison with existing results for the TCR-free case. We conduct several numerical experiments to illustrate the theoretical findings in Section 4 and draw conclusions in Section 5.

2. Robin-Schwarz algorithm and its convergence

The Schwarz method with a standard Robin transmission condition for solving model problem (1.1) involves iteratively solving subproblems on Ω_i, $i = 1, 2$, with Robin conditions updated using the solutions from the adjacent subproblems obtained in the previous iteration. More specifically, the iterative scheme with a Robin parameter p for the n-th iteration is expressed as follows:

$$\begin{cases} (c_1 - \kappa_1\Delta)T_1^n = f & \text{in } \Omega_1, \\ T_1^n = 0 & \text{on } \partial\Omega_1\backslash\Gamma, \\ \kappa_1\nabla T_1^n \cdot \mathbf{n_1} + pT_1^n = g_1^{n-1} & \text{on } \Gamma, \end{cases} \tag{2.1}$$

and

$$\begin{cases} (c_2 - \kappa_2\Delta)T_2^n = f & \text{in } \Omega_2, \\ T_2^n = 0 & \text{on } \partial\Omega_2\backslash\Gamma_2, \\ \kappa_2\nabla T_2^n \cdot \mathbf{n_2} + pT_2^n = g_2^{n-1} & \text{on } \Gamma, \end{cases} \tag{2.2}$$

where g_1^{n-1} and g_2^{n-1} are defined as

$$\begin{cases} g_1^{n-1} = (pR_c - 1)\kappa_2\nabla T_2^{n-1} \cdot \mathbf{n_2} + pT_2^{n-1} & \text{on } \Gamma, \\ g_2^{n-1} = (pR_c - 1)\kappa_1\nabla T_1^{n-1} \cdot \mathbf{n_1} + pT_1^{n-1} & \text{on } \Gamma, \end{cases} \tag{2.3}$$

which can be updated in the following way:

$$\begin{cases} g_1^{n-1} = \left(2p - p^2R_c\right)T_2^{n-2} + (pR_c - 1)g_2^{n-2} & \text{on } \Gamma, \\ g_2^{n-1} = \left(2p - p^2R_c\right)T_1^{n-2} + (pR_c - 1)g_1^{n-2} & \text{on } \Gamma, \end{cases} \tag{2.4}$$

and consequently, there is no need to reconstruct gradient information from the numerical data.

The Robin-Schwarz algorithm (2.1)–(2.4) is well-posed and its convergence for any positive Robin parameter $p > 0$ can be proved using the energy estimate; cf. [24]. Unfortunately, the energy estimate does not provide any insight into the rate of convergence.

2.1. Convergence factor

To describe the convergence rate of the Robin-Schwarz algorithm (2.1)–(2.4), we investigate the corresponding convergence factor using Fourier analysis. To this end, we consider the two-dimensional problem and assume that the defining domain is infinite, $\Omega = \Omega_1 \cup \Omega_2$, where $\Omega_1 := (-\infty, 0) \times \mathbb{R}$, $\Omega_2 := (0, \infty) \times \mathbb{R}$. It is evident that the normal vectors are $\boldsymbol{n_1} = (1, 0), \boldsymbol{n_2} = (-1, 0)$. By linearity, it suffices to consider the case when $f = 0$ and to analyze the convergence to zero. Applying a Fourier transform in the y direction for both Eqs (2.1) and (2.2) results in the following transformed system:

$$\begin{cases} (-\kappa_1 \partial_{xx} + c_1 + \kappa_1 k^2)\hat{T}_1^n = 0 & x \in (-\infty, 0), \\ (\kappa_1 \partial_x + p)\hat{T}_1^n = ((1 - pR_c)\kappa_2 \partial_x + p)\hat{T}_2^{n-1} & x = 0, \end{cases} \tag{2.5}$$

$$\begin{cases} (-\kappa_2 \partial_{xx} + c_2 + \kappa_2 k^2)\hat{T}_2^n = 0 & x \in (0, +\infty), \\ (-\kappa_2 \partial_x + p)\hat{T}_2^n = ((-1 + pR_c)\kappa_1 \partial_x + p)\hat{T}_1^{n-1} & x = 0, \end{cases} \tag{2.6}$$

where k denotes the Fourier frequency. Solving the first equations in (2.5) and (2.6), one then finds that the basic solutions meeting the requirement of boundedness are given by $\hat{T}_1^n = A_1^n e^{\lambda_1(k)x}$, $\hat{T}_2^n = B_2^n e^{-\lambda_2(k)x}$ with $\lambda_i(k) = \frac{\sqrt{c_i \kappa_i + \kappa_i^2 k^2}}{\kappa_i}$ being the characteristic roots of the first equations in (2.5) and (2.6). Inserting them into the Fourier transformed transmission conditions in (2.5) and (2.6), and iterating between the subdomains, we derive the convergence factor, after a simplification, as

$$\rho(k, p) = \frac{(1 - pR_c) - p\xi_2(k)}{1 + p\xi_1(k)} \cdot \frac{(1 - pR_c) - p\xi_1(k)}{1 + p\xi_2(k)}, \tag{2.7}$$

where

$$\xi_1(k) = \frac{1}{\kappa_1 \lambda_1(k)}, \quad \xi_2(k) = \frac{1}{\kappa_2 \lambda_2(k)}.$$

Note that the convergence factor ρ is symmetric in k, i.e., $\rho(k, p) = \rho(-k, p)$. To optimize the convergence performance of the Robin-Schwarz algorithm (2.1)–(2.4), one can then determine the optimal parameter p by minimizing the maximum of the convergence factor ρ over the specific positive frequencies $k \in [k_{min}, k_{max}]$, which leads to the following optimization problem:

$$\min_{p \in \mathbb{R}^+} \max_{k \in [k_{min}, k_{max}]} |\rho(k, p)|, \tag{2.8}$$

where k_{min} denotes the smallest frequency that is involved in the calculation and k_{max} denotes the largest one. In general, k_{min} is estimated as $\pi/|\Gamma|$, while k_{max} is estimated as π/h when a uniform mesh of size h is applied [25].

3. Optimization

For the min-max optimization problem (2.8) involving the two variables $p > 0$ and k, the objective is to minimize the maximum of the convergence factor over all Fourier frequencies $k \in [k_{min}, k_{max}]$. To

systematically analyze this problem, we introduce the following series of lemmas to restrict the range of the parameter p and determine the extremal behavior of the convergence factor with respect to the frequency k.

Lemma 1. *Assume that $\kappa_i > 0$ and $c_i \geq 0$ for $i = 1, 2$. The functions $\xi_i(k)$ are positive and monotonically decrease in k for $k > 0$.*

Proof. The positivity of $\xi_i(k)$ is obvious and the decreasing property can be obtained by checking the sign of the derivative $\frac{\partial \xi_i(k)}{\partial k}$. □

First, restrict the range of optimization for parameter p.

Lemma 2 (Restricting the range for p)**.** *Assume that $R_c, \kappa_i > 0$ and $c_i \geq 0$ for $i = 1, 2$. If the parameter p^* is a solution to the min-max problem* (2.8)*, then p^* must lie within the interval $I := [\min\{p_1(k_{min}), p_2(k_{min})\}, \max\{p_1(k_{max}), p_2(k_{max})\}]$, where the functions*

$$p_1(k) = \frac{1}{R_c + \xi_1(k)}, \ p_2(k) = \frac{1}{R_c + \xi_2(k)} \tag{3.1}$$

are zeros of ρ. Thus, the min-max problem (2.8) *is equivalently reduced to the following problem:*

$$\min_{p \in I} \max_{k \in [k_{min}, k_{max}]} |\rho(k, p)|. \tag{3.2}$$

Proof. The derivative of $\rho(k, p)$ with respect to p is given by

$$\frac{\partial \rho(k, p)}{\partial p} = \frac{(R_c + \xi_1(k) + \xi_2(k))(p^2(R_c + 2\xi_2(k))\xi_1(k) + p^2 R_c \xi_2(k) + 2pR_c - 2)}{(1 + p\xi_1(k))^2(1 + p\xi_2(k))^2}.$$

Setting $\frac{\partial \rho}{\partial p} = 0$, we obtain the minimum point $\overline{p}(k)$ of the convergence factor ρ with respect to p:

$$\overline{p}(k) = \frac{2}{R_c + \sqrt{(2\xi_1(k) + R_c)(2\xi_2(k) + R_c)}}. \tag{3.3}$$

With all physical parameters held constant, the functions $\xi_1(k)$ and $\xi_2(k)$ can be directly compared at the same k-values. Assuming without loss of generality that $\xi_1(k) > \xi_2(k)$, this implies the inequality $p_1(k) < \overline{p}(k) < p_2(k)$. We will show that $p^* \in I$ by contradiction. Suppose that $p \notin I = [p_1(k_{min}), p_2(k_{max})]$. Then, for all $k \in [k_{min}, k_{max}]$, we have $|\rho(k, p)| = \rho(k, p)$. If $p < p_1(k_{min}) < \overline{p}(k)$, it follows that $\frac{\partial \rho}{\partial p}(k, p) < 0$ for all $k \in [k_{min}, k_{max}]$. Hence, increasing p results in a uniform decrease in $\rho(k, p)$ in all k. In contrast, if $p > p_2(k_{max}) > \overline{p}(k)$, we find that $\frac{\partial \rho}{\partial p}(k, p) > 0$ for all $k \in [k_{min}, k_{max}]$. In this scenario, decreasing p also leads to a uniform decrease in $\rho(k, p)$ in all k. Therefore, if p^* is a solution to (2.8), it cannot be less than $p_1(k_{min})$ or greater than $p_2(k_{max})$. □

Convergence is guaranteed for any parameter p within the constrained range.

Theorem 1. *For all $p \in I$, it holds that $pR_c < 1$, which leads to $|\rho(k, p)| < 1$, i.e., the Schwarz iteration defined by Eqs* (2.1)–(2.4) *converges.*

Proof. From the expression (3.1), one finds for $i = 1, 2$ that $p_i(k)R_c < 1$ holds for any $k \in [k_{\min}, k_{\max}]$ because of the positivity of $\xi_i(k)$ and $\xi_2(k)$ (cf. Lemma 1). Hence, for any $p \in I$, we have $pR_c < 1$, which implies $|\rho(k, p)| < 1$ by a direct calculation. □

Second, to solve the maximization subproblem in the min-max formulation (3.2), determine the global maximum of the convergence factor over all related Fourier frequencies.

Lemma 3 (Local maxima in k)**.** *Let $R_c, \kappa_i > 0$ and $c_i \geq 0$ for $i = 1, 2$. For any $p \in I$, the maximum of the function $|\rho(k, p)|$ over $k \in [k_{min}, k_{max}]$ satisfies*

$$\begin{aligned} &\max_{k\in[k_{min},k_{max}]} |\rho(k,p)| \\ &= \begin{cases} \max\{\rho(k_{min},p), \rho(k_{max},p)\} & \text{if } \overline{k} \notin [k_{min}, k_{max}], \\ \max\{\rho(k_{min},p), -\rho(\overline{k},p), \rho(k_{max},p)\} & \text{if } \overline{k} \in [k_{min}, k_{max}], \end{cases} \end{aligned} \tag{3.4}$$

where $\overline{k} \in (\min\{k_1(p), k_2(p)\}, \max\{k_1(p), k_2(p)\})$ is the minimum point of $\rho(k, p)$.

Proof. Define $\rho_i(k,p) := \frac{1-p(R_c+\xi_i(k))}{1+p\xi_i(k)}$. It follows that $\partial_k\rho_i(k,p) = pk\kappa_i(2 - R_cp)/\sqrt{k^2+\eta_i}(\kappa_i\sqrt{k^2+\eta_i}+p)^2 > 0$, with $\eta_i := \frac{c_i}{\kappa_i}, i = 1, 2$, which implies that both $\rho_i(k,p), i = 1, 2$, are monotonically increasing functions in k. The positive roots of $\rho_i(k,p)$ in k can be expressed as $k_i(p) = \frac{\sqrt{-\eta_i\kappa_i^2(R_cp-1)^2+p^2}}{(1-R_cp)\kappa_i}, i = 1, 2$. Without loss of generality, we assume $k_1(p) < k_2(p)$. Noting that $\rho(k,p) = \rho_1(k,p)\cdot\rho_2(k,p)$, the derivative of $\rho(k,p)$ in k is

$$\frac{\partial\rho}{\partial k} = \frac{\partial\rho_1(k,p)}{\partial k}\rho_2(k,p) + \frac{\partial\rho_2(k,p)}{\partial k}\rho_1(k,p). \tag{3.5}$$

For $k \in (0, k_1(p))$, we have $\rho_2(k,p) < \rho_1(k,p) < 0$, thereby implying that $\rho(k,p) > 0, \frac{\partial\rho}{\partial k} < 0$. Consequently, $\rho(k,p)$ is strictly decreasing in k.

For $k \in (k_2(p), \infty)$, it holds that $0 < \rho_2(k,p) < \rho_1(k,p)$. Thus $\rho(k,p) > 0, \frac{\partial\rho}{\partial k} > 0$, indicating that $\rho(k,p)$ is strictly increasing in k.

For $k \in (k_1(p), k_2(p))$, we find that $\rho(k,p) < 0$. By the continuity of $\rho(k,p)$, there exists at least one point $\overline{k}$ such that $\frac{\partial\rho(k,p)}{\partial k} = 0$ and $\rho(\overline{k},p) \leq \rho(k \neq \overline{k}, p)$ for all $k \in (k_1(p), k_2(p))$. Thus, the maximum of $|\rho(k,p)|$ is attained at $\overline{k}$, although an explicit expression for $\overline{k}$ cannot be derived.

We then conclude that the assertion (3.4) holds according to different positions of $\overline{k}$ for any given $p \in I$. □

Remark 1. *A fundamental challenge emerges when $R_c > 0$ and $c_i > 0$: the minimum point $\overline{k}$ admits no closed-form solution. Even when $R_c = 0$, the explicit form of $\overline{k}$ is prohibitively complex due to c_i, critically obstructing parameter optimization—an unsolved issue in existing analyses. To enable comparative analysis, this work therefore focuses on the special case when $c_i = 0$. For the specific case $R_c = c_i = 0$ [23], $\overline{k}$ is*

$$\overline{k} = \frac{p}{\sqrt{\kappa_1\kappa_2}},$$

which leads the convergence factor $|\rho(\overline{k},p)|$ at $\overline{k}$ to be parameter p independent. However, when $R_c > 0$ and $c_i = 0$, the minimum point $\overline{k}$ of $\rho(k,p)$ has the more-intricate closed form:

$$\overline{k} = \frac{\left(R_c\kappa_1\kappa_2 p + \sqrt{\kappa_1\kappa_2(R_c\kappa_1 p - \kappa_1 - \kappa_2)(R_c\kappa_2 p - \kappa_1 - \kappa_2)}\right)p}{\kappa_1\kappa_2(\kappa_1+\kappa_2)(1-R_cp)}. \tag{3.6}$$

This formulation induces critical consequence upon substituting $\overline{k}$ in (3.6) into $|\rho(\overline{k},p)|$: at $\overline{k}$, the convergence factor becomes p-dependent, challenging the analysis of how the maximum $|\rho(\overline{k},p)|$ behaves in p, essentially differing from the TCR-free case where $R_c = 0$.

According to Lemma 3, the maximum of the convergence factor may occur at three points $k_{min}, \overline{k}, k_{max}$. Given that analyzing the behavior of $|\rho(k, p)|$ at the internal maximum point with respect to p is complex, the following theorem will first study the variation of $|\rho(k, p)|$ at the endpoints k_{min}, k_{max} as p changes.

Theorem 2 (Equioscillation at the endpoints)**.** *The solution p^*_{lr} that minimizes the endpoint maximum*

$$\min_{p\in I} \max\{|\rho(k_{min}, p)|, |\rho(k_{max}, p)|\}$$

is determined by the equioscillation at the endpoints

$$|\rho(k_{min}, p)| = |\rho(k_{max}, p)|$$

and can be categorized as the following:

Case 1. $p_2(k_{min}) < p_1(k_{max})$. The solution p^*_{lr} corresponds to the unique solution of the equation

$$\rho(k_{min}, p) = \rho(k_{max}, p)$$

within the interval $(p_2(k_{min}), p_1(k_{max}))$. Refer to Figure 1.

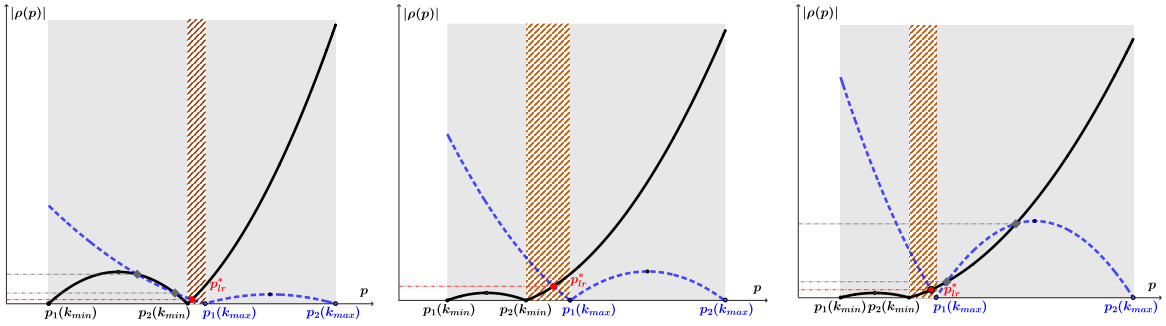

Figure 1. Convergence factors $|\rho(k_{min}, p)|$ (solid line) and $|\rho(k_{max}, p)|$ (dotted line) when $p_2(k_{min}) < p_1(k_{max})$.

Case 2. $p_2(k_{min}) > p_1(k_{max})$.

(i) If $|\rho(k_{min}, p)|$ does not intersect with $|\rho(k_{max}, p)|$ between the maxima $\overline{p}(k_{min})$ and $\overline{p}(k_{max})$, then p^*_{lr} is one of the solutions to

$$-\rho(k_{min}, p) = \rho(k_{max}, p)$$

within the interval $(p_1(k_{min}), p_1(k_{max})) \cup (p_2(k_{min}), p_2(k_{max}))$ that corresponds to the smallest convergence factor. Refer to the top row of Figure 2.

(ii) Conversely, if $|\rho(k_{min}, p)|$ intersects with $|\rho(k_{max}, p)|$ between the maxima $\overline{p}(k_{min})$ and $\overline{p}(k_{max})$, then p^*_{lr} is determined either by the unique solution to the equation

$$\rho(k_{min}, p) = \rho(k_{max}, p)$$

in the interval $(\max\{p_1(k_{max}), \overline{p}(k_{min})\}, \min\{\overline{p}(k_{max}), p_2(k_{min})\})$, or by one of the solutions to the equation

$$-\rho(k_{min}, p) = \rho(k_{max}, p)$$

in the interval $(p_1(k_{min}), \min\{p_1(k_{max}), \overline{p}(k_{min})\}) \cup (\max\{\overline{p}(k_{max}), p_2(k_{min})\}, p_2(k_{max}))$ that corresponds to the smallest convergence factor. Refer to the bottom row of Figure 2.

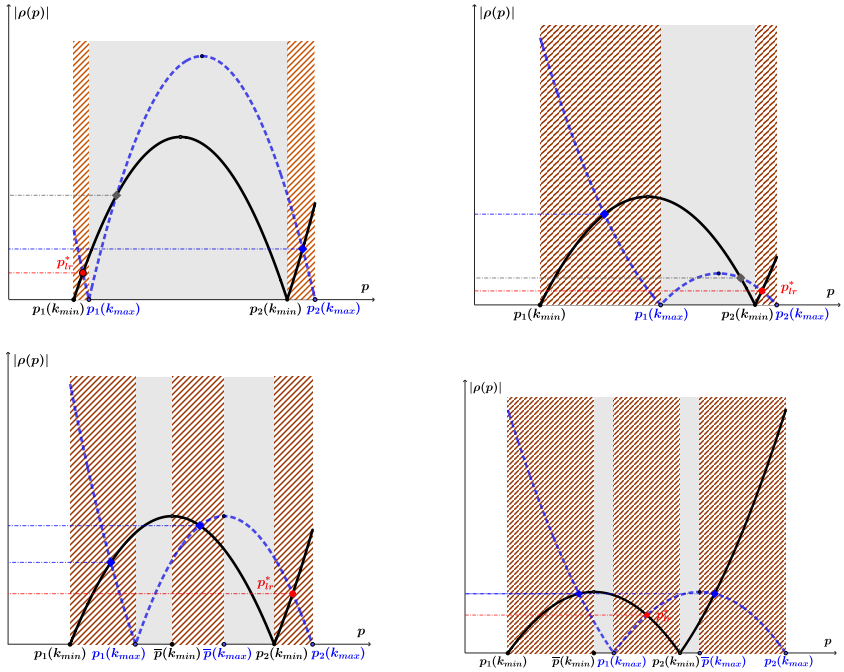

Figure 2. The convergence factors for $|\rho(k_{min}, p)|$ (solid line) and $|\rho(k_{max}, p)|$ (dotted line) when $p_2(k_{min}) > p_1(k_{max})$.

The proof of Theorem 2, being rather lengthy, is deferred to the Appendix. Theorem 2 implies that p_{lr}^* is the solution to the endpoint equioscillation equation $|\rho(k_{min}, p)| = |\rho(k_{max}, p)|$ (i.e., $\rho(k_{min}, p) = \rho(k_{max}, p)$ or $-\rho(k_{min}, p) = \rho(k_{max}, p)$), and this solution minimizes the endpoint convergence factor. Building upon this, Theorem 3 further shows that when the system satisfies specific conditions, the parameter p_{lr}^* determined by endpoint equioscillation is precisely the global optimal solution to the min-max problem (2.8). Specifically, if p_{lr}^* is directly determined by the equation $\rho(k_{min}, p) = \rho(k_{max}, p)$, then an explicit closed-form solution exists, and an asymptotic expression can be derived.

Theorem 3 (Optimized Robin condition)**.** *The parameter p_{lr}^* defined in Theorem 2 is the solution of the min-max problem* (2.8) *if $\overline{k} \notin [k_{min}, k_{max}]$, or $\overline{k} \in [k_{min}, k_{max}]$ but $|\rho(\overline{k}, p_{lr}^*)| \le |\rho(k_{min}, p_{lr}^*)|$.*

When determined by $\rho(k_{min}, p) = \rho(k_{max}, p)$, p_{lr}^* is explicitly given by

$$p_{lr}^* = \frac{R_c\phi_1 - \sqrt{\phi_2\phi_4}}{\phi_3}, \tag{3.7}$$

with $\phi_1 := (\xi_1(k_{min}) + \xi_2(k_{min}) - \xi_1(k_{max}) - \xi_2(k_{max}))$, $\phi_2 := \xi_1(k_{max}) + \xi_2(k_{max}) - \xi_1(k_{min}) - \xi_2(k_{min})$, $\phi_3 := -2\xi_1(k_{min})\xi_2(k_{min})(R_c + 2\xi_2(k_{max})) + ((2\xi_2(k_{max}) - 2\xi_2(k_{min}))\xi_1(k_{min}) + 2\xi_2(k_{max})(R_c + \xi_2(k_{min})))\xi_1(k_{max})$, $\phi_4 := ((4\xi_2(k_{max}) - 4\xi_2(k_{min}))\xi_1(k_{min}) + (4R_c + 4\xi_2(k_{min}))\xi_2(k_{max}) + R_c^2)\xi_1(k_{max}) + (-4\xi_2(k_{max})\xi_2(k_{min}) - R_c(R_c + 4\xi_2(k_{min})))\xi_1(k_{min}) + R_c^2(\xi_2(k_{max}) - \xi_2(k_{min}))$.

For $k_{max} = \frac{\pi}{h}$ and h sufficiently small, a Taylor expansion with respect to h gives

$$p_{lr}^* = \frac{\hat{\varphi}_1}{2R_c} + O(h), \quad \rho(k_{min}, p_{lr}^*) = (1 - \frac{\hat{\varphi}_1}{2})^2 + O(h), \tag{3.8}$$

where

$$\hat{\varphi}_1 = \hat{\varphi}_2 - R_c(\hat{\varphi}_3(k_{min})\kappa_1 + \hat{\varphi}_4(k_{min})\kappa_2),$$
$$\hat{\varphi}_2 = \sqrt{R_c(4 + R_c(\hat{\varphi}_3(k_{min})\kappa_1 + \hat{\varphi}_4(k_{min})\kappa_2))(\hat{\varphi}_3(k_{min})\kappa_1 + \hat{\varphi}_4(k_{min})\kappa_2)},$$
$$\hat{\varphi}_3(x) = \sqrt{x^2 + \eta_1},\ \hat{\varphi}_4(x) = \sqrt{x^2 + \eta_2}.$$

Proof. The results can be established through direct calculations. □

Remark 2. *The min-max problem described in Eq* (2.8) *is addressed by the parameter p^*_{lr} only under specific cases; thus, it is not completely resolved in Theorem 2. The complete result is presented below, although its practical applicability may be limited.*

(1) If $\overline{k} \notin [k_{min}, k_{max}]$, or if $\overline{k} \in [k_{min}, k_{max}]$ but $|\rho(\overline{k}, p^*_{lr})| \leq |\rho(k_{min}, p^*_{lr})|$, then we have $p^* = p^*_{lr}$.

(2) Conversely, if the above conditions are not satisfied, the solution p^* to the min-max problem (2.8) *resides within the set $S = S_{lc} \cup S_{cr}$, with $S_{lc} := \{p^*_{lc} \mid |\rho(k_{min}, p^*_{lc})| = |\rho(\overline{k}, p^*_{lc})|\}$ and $S_{cr} := \{p^*_{cr} \mid |\rho(k_{max}, p^*_{cr})| = |\rho(\overline{k}, p^*_{cr})|\}$, and $p^* = \min_{p\in S} \max\{|\rho(k_{min}, p)|, |\rho(\overline{k}, p)|, |\rho(k_{max}, p)|\}$.*

In other words, the solution to the min-max problem (2.8) *must be one of the solutions to the three equioscillation equations $|\rho(k_{min}, p)| = |\rho(k_{max}, p)|$, $|\rho(k_{min}, p)| = |\rho(\overline{k}, p)|$, and $|\rho(\overline{k}, p)| = |\rho(k_{max}, p)|$, and this solution minimizes the maximum of the convergence factor. Therefore, if $\rho(\overline{k}, p)$ is explicitly defined ($c_i = 0$), then p^* can be determined accordingly; otherwise, an estimation of p^* can be made using p^*_{lr}.*

Figure 3 depicts the behavior of $|\rho(k_{min}, p)|, |\rho(\overline{k}, p)|, |\rho(k_{max}, p)|$ with respect to $p \in I$ given the parameters $\kappa_1 = 2, \kappa_2 = 2000, c_1 = c_2 = 0, R_c = 0.001$, and the intersection points of p. It also presents the convergence factor $|\rho(k, p)|$ as a function of k at these points. We observe that under specific parameter values, there exist at most three equioscillation scenarios, and the solution $p^* = 922.8704258$ of the min-max problem is determined by one of them.

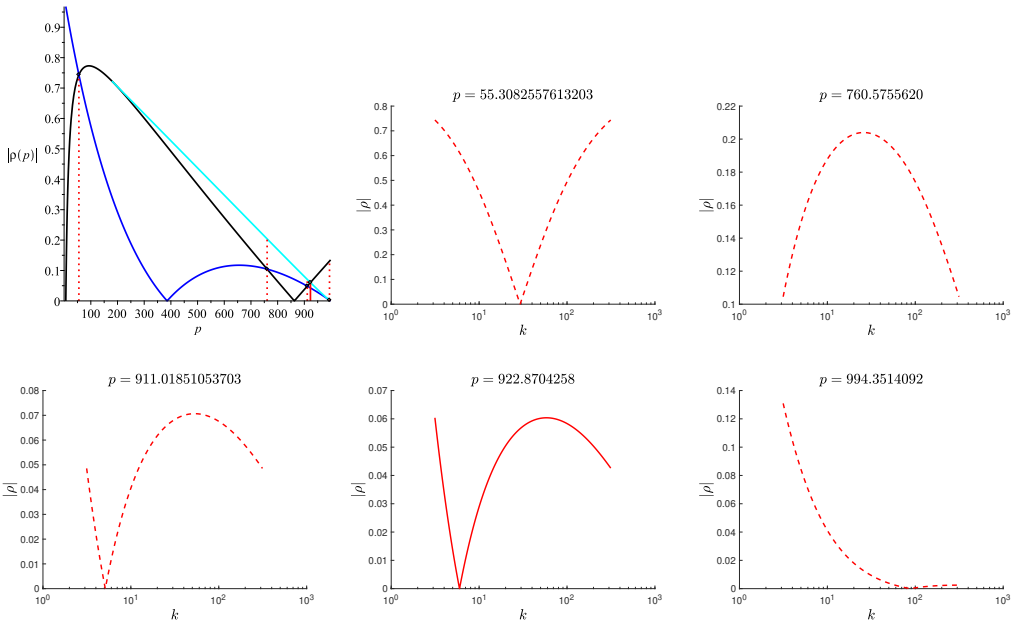

Figure 3. Subfigure 1: Convergence factors $|\rho(k_{min}, p)|$ (black line), $|\rho(\overline{k}, p)|$ (cyan line), $|\rho(k_{max}, p)|$ (blue line) as functions of p, along with their intersection points. Remaining subfigures: Convergence factors at different intersection points of the first subfigure, plotted as functions of k.

Building on previous analysis, the impact of physical parameters on the convergence rate is further explored.

Remark 3. *In the special case where $c_i = 0, i = 1, 2$, when the TCR is disregarded, i.e., $R_c = 0$, it has been demonstrated in [23] that heterogeneity contrast negatively impacts the convergence of the OSM. Specifically, a greater contrast results in slower convergence rates. Conversely, when the TCR is present, $R_c > 0$, we observe an opposite phenomenon: a larger heterogeneity contrast facilitates faster convergence of the OSM. To elucidate this relationship, we define the heterogeneity contrast as $\lambda := \frac{\kappa_1}{\kappa_2}$. Now, by symmetry, we can restrict our analysis to the case where $\kappa_1 \geq \kappa_2$, i.e., $\lambda \geq 1$. Reformulating the estimate in* (3.8) *and expanding for large λ yields*

$$\max_{k_{min} \leq k \leq \frac{\pi}{h}} |\rho(k, p_{lr}^*)| = \frac{1}{(R_c \kappa_2 k_{min})^2} \cdot \frac{1}{\lambda^2} + O(\frac{1}{\lambda^3}) + O(h). \tag{3.9}$$

This result corroborates our previous assertion for a fixed value of κ_2. Furthermore, Eq (3.9) *indicates that, for fixed heterogeneity contrast λ, an increase in the thermal conductivity κ_i leads to accelerated convergence. This behavior is notably absent in scenarios where the TCR is not considered.*

Remark 4. *Now we investigate the influence of R_c on convergence behavior. For fixed $\kappa_i, c_i, i = 1, 2$, Taylor expanding the convergence factor at $R_c = 0$ yields*

$$\rho(k_{min}, p^*) = 1 - 2\sqrt{\kappa_1 \hat{\varphi}_3(k_{min}) + \kappa_2 \hat{\varphi}_4(k_{min})} R_c^{\frac{1}{2}} + O(R_c). \tag{3.10}$$

This indicates that convergence deteriorates as R_c decreases, as anticipated. Furthermore, we can infer from Eq (3.9) *that a larger TCR enhances convergence quadratically.*

4. Numerical experiments

To demonstrate our theoretical findings, we solve the heat conduction problem (1.1) on the domain $\Omega = (0, 1)^2$ consisting of two subdomains $\Omega_1 = (-1, 0) \times (0, 1)$ and $\Omega_2 = (0, 1) \times (0, 1)$, with interface $\Gamma = \{0\} \times (0, 1)$. The problem is solved using the OSM algorithm (2.1)–(2.4), discretized with standard centered finite difference on a uniform grid of size h.

Random initial guesses $g_{1,2}$ on Γ are used to initiate the iteration.

To verify the convergence order of the scheme, consider the exact solutions $T_1 = \frac{\kappa_2}{\kappa_1} x \sin(\pi x) \sin(\pi y)$ and $T_2 = x \sin(\pi x) \sin(\pi y)$, which satisfy Eq (1.1) with $\kappa_1 = 2, \kappa_2 = 0.01, R_c = 0.01$, and $c_1 = c_2 = 0$. In Figure 4, we plot the error against the mesh size h, which shows second-order convergence as expected.

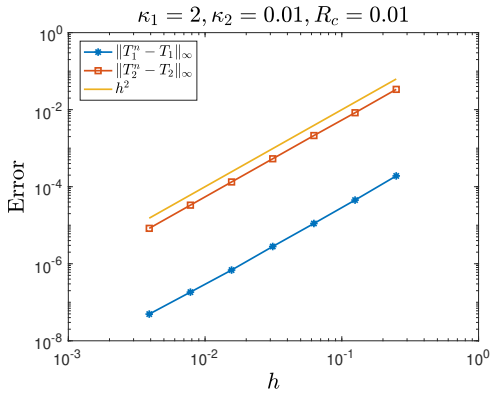

Figure 4. Error as a function of mesh size h.

To illustrate our theoretical results, we consider the homogeneous heat conduction problem (1.1) with $f = 0$, which means that we solve the error equation directly. Now, the OSM algorithm (2.1)–(2.4) terminates when the maximum errors fall below the tolerance *tol*,

$$\max\{\|T_1^n\|_\infty, \|T_2^n\|_\infty\} < tol,$$

where T_i^n are the numerical solutions at the n-th iteration, representing the error since the exact solution is zero.

To demonstrate the mesh-independent convergence rate estimates presented in Theorem 3, as well as the influence of heterogeneous contrast and the diffusion coefficient on the algorithm as discussed in Remark 3, we present in Table 1 the number of iterations required by the OSM algorithm (2.1)–(2.4) to achieve the tolerance criterion $tol = 10^{-6}$. The results are reported for various mesh sizes h, heterogeneous contrasts λ, and diffusion coefficients (κ_1, κ_2). The optimal parameters used in the experiments are derived from Remark 2. The results indicate that the number of iterations remains constant across different mesh sizes, confirming the mesh independence of the algorithm. Furthermore, for a fixed κ_2, larger heterogeneous contrasts accelerate the convergence of the algorithm. This observation contrasts with the findings using optimized parameters in [23] when $R_c = 0$. Similarly, larger diffusion coefficients also contribute to faster convergence. Figure 5 shows that optimized parameters in Remark 2 predict very well the optimal transmission parameters.

Table 1. Iteration counts for various mesh sizes, heterogeneity contrast, and thermal conductivity for $c_1 = c_2 = 0, R_c = 0.01$ (iteration counts corresponding to $R_c = 0$ are listed in parenthesis).

$\kappa_1 = 2, \kappa_2 = 0.01$		$\kappa_2 = 0.01, h = \frac{1}{512}$		$h = \frac{1}{512}$	
h	iters	λ	iters	(κ_1, κ_2)	iters
$\frac{1}{32}$	20	2	69(72)	$(2, 1)$	17
$\frac{1}{64}$	21	$2 \cdot 10^1$	28(30)	$(2, 1) \cdot 10^1$	6
$\frac{1}{128}$	21	$2 \cdot 10^2$	21(37)	$(2, 1) \cdot 10^2$	3
$\frac{1}{256}$	21	$2 \cdot 10^3$	9(104)	$(2, 1) \cdot 10^3$	2
$\frac{1}{512}$	21	$2 \cdot 10^4$	4(288)	$(2, 1) \cdot 10^4$	2

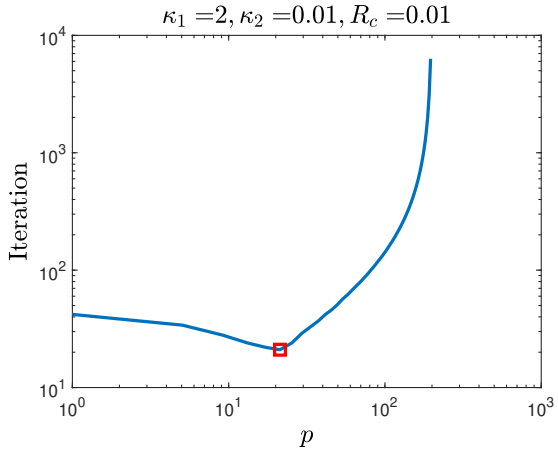

Figure 5. Number of iterations required by the algorithm (2.1)–(2.4) using a mesh size $h = \frac{1}{256}$ as a function of transmission parameter p. "□" indicates the theoretical result from Remark 2.

Next, we further examine how the magnitude of TCR affects convergence. According to Remark 4, a larger TCR R_c results in smaller convergence factors. To illustrate this, we record the number of iterations required by the algorithm (2.1)–(2.4) for varying R_c in Table 2. Furthermore, a large TCR also facilitates optimal convergence behavior, allowing the algorithm to converge in two iterations.

Table 2. Number of iterations required by the algorithm (2.1)–(2.4) to reach a tolerance of 10^{-6} for $\kappa_1 = 2, \kappa_2 = 0.01$, and $h = \frac{1}{512}$.

R_c	10^{-3}	10^{-2}	10^{-1}	10^{0}	10^{1}	10^{2}	10^{3}
iters	31	21	10	5	3	3	2

5. Conclusions

This study explores the use of the standard Robin transmission condition within the OSM framework for heat conduction in composite materials, focusing on the impact of TCR, which more accurately represents the physical behavior of such systems. Incorporating TCR significantly alters the performance of OSM algorithms compared to the TCR-absent case. Specifically, convergence becomes mesh-independent in the asymptotic limit when TCR is included, whereas it remains mesh-dependent without TCR. Moreover, factors such as large heterogeneity contrast, high thermal conductivity, and significant TCR magnitudes notably improve convergence rates. These effects contrast sharply with the scenario without TCR, where increased heterogeneity hampers convergence and conductivity has no impact. Numerical experiments validate these theoretical results.

Author contributions

Huan Zhang: Conceptualization, Formal analysis, Investigation, Methodology, Software, Visualization, Validation, Writing–original draft and editing; Yingxiang Xu: Conceptualization, Formal analysis, Investigation, Methodology, Supervision, Project administration, Validation, and Writing–review and editing. All authors have read and approved the final version of the manuscript for

publication.

Use of Generative-AI tools declaration

The authors declare that they have not used Artificial Intelligence (AI) tools in the creation of this article.

Acknowledgments

The authors thank the anonymous reviewers for their constructive comments. This work is supported by the Jilin Province Department of Education under the grant JJKH20250297BS.

Conflict of interest

There is no known conflict of interest associated with this publication.

References

1. P. D. Mangalgiri, Composite materials for aerospace applications, *Bull. Mater. Sci.*, **22** (1999), 657–664. https://doi.org/10.1007/BF02749982
2. C. Zweben, Advances in composite materials for thermal management in electronic packaging, *JOM*, **50** (1998), 47–51. https://doi.org/10.1007/s11837-998-0128-6
3. J. I. Frankel, B. Vick, M. N. Özisik, General formulation and analysis of hyperbolic heat conduction in composite media, *Int. J. Heat Mass Transfer*, **30** (1987), 1293–1305. https://doi.org/10.1016/0017-9310(87)90162-1
4. P. L. Kapitza, Heat transfer and superfluidity of helium II, *Phys. Rev.*, **60** (1941), 354. https://doi.org/10.1103/PhysRev.60.354
5. O. M. Necati, *Heat conduction*, John Wiley & Sons, Inc, 1993.
6. E. T. Swartz, R. O. Pohl, Thermal boundary resistance, *Rev. Mod. Phys.*, **61** (1989), 605. https://doi.org/10.1103/RevModPhys.61.605
7. P. K. Jain, S. Singh, Rizwan-uddin, An exact analytical solution for two-dimensional, unsteady, multilayer heat conduction in spherical coordinates, *Int. J. Heat Mass Transfer*, **53** (2010), 2133–2142. https://doi.org/10.1016/j.ijheatmasstransfer.2009.12.035
8. S. Singh, P. K. Jain, Rizwan-uddin, Finite integral transform method to solve asymmetric heat conduction in a multilayer annulus with time-dependent boundary conditions, *Nucl. Eng. Des.*, **241** (2011), 144–154. https://doi.org/10.1016/j.nucengdes.2010.10.010
9. A. Amiri Delouei, M. Norouzi, Exact analytical solution for unsteady heat conduction in fiber-reinforced spherical composites under the general boundary conditions, *J. Heat Transfer*, **137** (2015), 101701. https://doi.org/10.1115/1.4030348
10. Y. Gong, B. Li, Z. Li, Immersed-interface finite-element methods for elliptic interface problems with nonhomogeneous jump conditions, *SIAM J. Numer. Anal.*, **46** (2008), 472–495. https://doi.org/10.1137/060666482

11. M. Oevermann, R. Klein, A Cartesian grid finite volume method for elliptic equations with variable coefficients and embedded interfaces, *J. Comput. Phys.*, **219** (2006), 749–769. https://doi.org/10.1016/j.jcp.2006.04.010
12. R. Massjung, An unfitted discontinuous Galerkin method applied to elliptic interface problems, *SIAM J. Numer. Anal.*, **50** (2012), 3134–3162. https://doi.org/10.1137/090763093
13. H. Ji, F. Wang, J. Chen, Unfitted finite element methods for the heat conduction in composite media with contact resistance, *Numer. Methods Partial Differ. Equ.*, **33** (2017), 354–380. https://doi.org/10.1002/num.22111
14. L. Wang, S. Hou, L. Shi, A weak formulation for solving the elliptic interface problems with imperfect contact, *Adv. Appl. Math. Mech.*, **9** (2017), 1189–1205. https://doi.org/10.4208/aamm.2015.m1236
15. F. Cao, Z. Sheng, G. Yuan, Monotone finite volume schemes for diffusion equation with imperfect interface on distorted meshes, *J. Sci. Comput.*, **76** (2018), 1055–1077. https://doi.org/10.1007/s10915-018-0651-8
16. M. J. Gander, V. Martin, An introduction to heterogeneous domain decomposition methods for multi-physics problems, In: *Domain decomposition methods in science and engineering XXVII*, Lecture Notes in Computational Science and Engineering, Springer, 2022, 215–222. https://doi.org/10.1007/978-3-031-50769-4_25
17. M. J. Gander, Optimized Schwarz methods, *SIAM J. Numer. Anal.*, **44** (2006), 699–731. https://doi.org/10.1137/S0036142903425409
18. M. J. Gander, T. Vanzan, Heterogeneous optimized Schwarz methods for coupling Helmholtz and Laplace equations, In: *Domain decomposition methods in science and engineering XXIV*, Lecture Notes in Computational Science and Engineering, Springer, 2018, 311–320. https://doi.org/10.1007/978-3-319-93873-8_29
19. M. Discacciati, L. Gerardo-Giorda, Is minimising the convergence rate a good choice for efficient Optimized Schwarz preconditioning in heterogeneous coupling? The Stokes-Darcy case, In: *Domain decomposition methods in science and engineering XXIV*, Lecture Notes in Computational Science and Engineering, Springer, 2018, 233–241. https://doi.org/10.1007/978-3-319-93873-8_21
20. M. J. Gander, T. Vanzan, Multilevel optimized Schwarz methods, *SIAM J. Sci. Comput.*, **42** (2020), A3180–A3209. https://doi.org/10.1137/19M1259389
21. Y. Liu, Y. Boubendir, X. He, Y. He, New optimized Robin–Robin domain decomposition methods using Krylov solvers for the Stokes–Darcy system, *SIAM J. Sci. Comput.*, **44** (2022), B1068–B1095. https://doi.org/10.1137/21M1417223
22. M. J. Gander, T. Vanzan, Heterogeneous optimized Schwarz methods for second order elliptic PDEs, *SIAM J. Sci. Comput.*, **41** (2019), A2329–A2354. https://doi.org/10.1137/18M122114X
23. M. J. Gander, O. Dubois, Optimized Schwarz methods for a diffusion problem with discontinuous coefficient, *Numer. Algor.*, **69** (2015), 109–144. https://doi.org/10.1007/s11075-014-9884-2
24. H. Zhang, H. Zhang, Y. Wang, Y. Xu, Heterogeneous optimized Schwarz methods for heat conduction in composites with thermal contact resistance, submitted for publication.
25. W. A. Strauss, *Partial differential equations: an introduction*, 2 Eds., John Wiley & Sons, 2007.

Appendix

Proof of Theorem 2

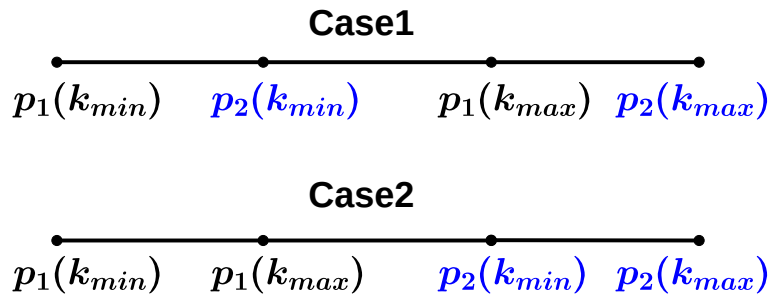

Figure A. Diagram of the positional relationship for $p_i(k), k = k_{kmin}, k_{max}, i = 1, 2$.

Proof. To analyze the monotonicity of the endpoint convergence factor with respect to the parameter p, we assume $\xi_1(k) < \xi_2(k)$ without loss of generality. The functions $p_i(k)$ defined by Eq (3.1) then satisfy $p_1(k) < p_2(k)$, implying: $p_1(k_{\min}) < p_2(k_{\min})$ and $p_1(k_{\max}) < p_2(k_{\max})$. By Lemma 2, the solution to the min-max problem (2.8) must lie within the interval $I = [p_1(k_{\min}), p_2(k_{\max})]$. However, the relationship $p_1(k_{\max}) < p_2(k_{\min})$ remains undetermined, leading to the two cases illustrated in Figure A. We now analyze the monotonicity of $|\rho(k_{\min}, p)|$ and $|\rho(k_{\max}, p)|$ for these two cases.

Case 1: $p_2(k_{\min}) < p_1(k_{\max})$

Refer to Figure 1. The parameter p exhibits distinct behaviors in three intervals:

- Interval $I_1 = [p_1(k_{\min}), p_2(k_{\min})]$:
  - $|\rho(k_{\max}, p)|$ strictly decreases.
  - $|\rho(k_{\min}, p)|$ increases from 0 to $\max\limits_{p} |\rho(k_{\min}, p)|$ at $\overline{p}(k_{\min})$, and then decreases to 0.
- Interval $I_2 = [p_2(k_{\min}), p_1(k_{\max})]$:
  - $|\rho(k_{\min}, p)|$ strictly increases from 0 to its maximum at $p_1(k_{\max})$.
  - $|\rho(k_{\max}, p)|$ strictly decreases to 0.
- Interval $I_3 = [p_1(k_{\max}), p_2(k_{\max})]$:
  - $|\rho(k_{\min}, p)|$ strictly increases.
  - $|\rho(k_{\max}, p)|$ increases from 0 to $\max\limits_{p} |\rho(k_{\max}, p)|$ at $\overline{p}(k_{\max})$, and then decreases to 0.

From this monotonicity, the parameter p that minimizes the endpoint convergence factor must satisfy the equioscillation condition ($|\rho(k_{\min}, p)| = |\rho(k_{\max}, p)|$) and correspond to the point with the smallest convergence factor value. Analysis of the intersection points reveals:

- I_1 contains at most two equioscillation points $p_l^*, \hat{p}_l^*$.
- I_2 contains a unique equioscillation point p_c^*.
- I_3 contains at most two equioscillation points $p_r^*, \hat{p}_r^*$.

By monotonicity, for any $p \in \{p_l^*, \hat{p}_l^*, p_r^*, \hat{p}_r^*\}$:

$$|\rho(k_{\min}, p_c^*)| \leq \max\left\{|\rho(k_{\min}, p)|,\ |\rho(k_{\max}, p)|\right\}.$$

Thus the optimal convergence occurs at $p_{lr}^* = p_c^*$ where:

$$\rho(k_{\min}, p_{lr}^*) = \rho(k_{\max}, p_{lr}^*).$$

Case 2: $p_2(k_{min}) > p_1(k_{max})$

Two subcases arise, depending on whether $|\rho(k_{min}, p)|$ and $|\rho(k_{max}, p)|$ intersect between their maxima $\overline{p}(k_{min})$ and $\overline{p}(k_{max})$.

(ii) No intersection between the maxima (top row of Figure 2), and we only demonstrate the proof for the first subfigure, with the other case being analogous.

Behavior in three intervals:

- Interval $I_1 = [p_1(k_{\min}), \overline{p}(k_{\min})]$:
  - $|\rho(k_{\min}, p)|$ strictly increases from 0 to $\max_p |\rho(k_{\min}, p)|$ at $\overline{p}(k_{\min})$.
  - $|\rho(k_{\max}, p)|$ decreases from $|\rho(k_{\max}, p_1(k_{\min}))| > 0$ to 0 at $p_1(k_{\max})$, and then increases to $|\rho(k_{\max}, \overline{p}(k_{\min}))| > |\rho(k_{\min}, \overline{p}(k_{\min}))|$.
- Interval $I_2 = [\overline{p}(k_{\min}), \overline{p}(k_{\max})]$:
  - $|\rho(k_{\min}, p)| \neq |\rho(k_{\max}, p)|$ for all p.
- Interval $I_3 = [\overline{p}(k_{\max}), p_2(k_{\max})]$:
  - $|\rho(k_{\max}, p)|$ strictly decreases from $\max_p |\rho(k_{\max}, p)|$ to 0.
  - $|\rho(k_{\min}, \overline{p}(k_{\max}))| < |\rho(k_{\max}, \overline{p}(k_{\max}))|$, and $|\rho(k_{\max}, p)|$ decreases to 0 at $p = p_2(k_{\min})$, and then increases to its maximum value $|\rho(k_{\min}, p_2(k_{\max}))| > 0$.

Analysis of the intersection points reveals:

- Two equioscillation points in I_1: $p_l^* \in (p_1(k_{\min}), p_1(k_{\max}))$ and $\hat{p}_l^* \in (p_1(k_{\max}), \overline{p}(k_{\min}))$ with $|\rho(k_{\min}, \hat{p}_l^*)| > |\rho(k_{\min}, p_l^*)|$.
- One equioscillation point in I_3: p_r^*.

The endpoint convergence factor minimizer p_{lr}^* is therefore

$$p_{lr}^* = \arg\min\{|\rho(k_{\min}, p_l^*)|, |\rho(k_{\min}, p_r^*)|\} \text{ subject to } \rho(k_{\min}, p_{lr}^*) = -\rho(k_{\max}, p_{lr}^*). \tag{.1}$$

(ii) Intersection between the maxima (bottom row of Figure 2).

Behavior in three intervals:

- Interval $I_1 = [p_1(k_{\min}), \min\{p_1(k_{\max}), \overline{p}(k_{\min})\}]$:
  - $|\rho(k_{\min}, p)|$ strictly increases to maximum at $p = \min\{p_1(k_{\max}), \overline{p}(k_{\min})\}$.
  - $|\rho(k_{\max}, p)|$ strictly decreases to 0 at $p_1(k_{\max})$.
- Interval $I_2 = [\max\{p_1(k_{\max}), \overline{p}(k_{\min})\}, \min\{\overline{p}(k_{\max}), p_2(k_{\min})\}]$:
  - $|\rho(k_{\min}, p)|$ strictly decreases.
  - $|\rho(k_{\max}, p)|$ strictly increases.
- Interval $I_3 = [\max\{\overline{p}(k_{\max}), p_2(k_{\min})\}, p_2(k_{\max})]$:
  - $|\rho(k_{\max}, p)|$ strictly decreases to 0.
  - $|\rho(k_{\min}, p)|$ strictly increases to maximum.

A unique equioscillation point exists in each subinterval:

$$p_l^* \in I_1, \quad p_c^* \in I_2, \quad p_r^* \in I_3.$$

The endpoint convergence factor minimizer p_{lr}^* satisfies:

$$\rho(k_{\min}, p_{lr}^*) = \rho(k_{\max}, p_{lr}^*) \quad \text{or} \quad \rho(k_{\min}, p_{lr}^*) = -\rho(k_{\max}, p_{lr}^*),$$

and is determined by:

$$p_{lr}^* = \arg\min\{|\rho(k_{\min}, p_l^*)|, |\rho(k_{\min}, p_c^*)|, |\rho(k_{\min}, p_r^*)|\}.$$

Case 3: $p_2(k_{\min}) = p_1(k_{\max})$
This case is impossible. □